An Electron Microscopic Study of Highly Oriented Undoped and $FeCl_3$-Doped Poly(*p*-phenylenevinylene)

X. B. Zhang,† G. Van Tendeloo, J. Van Landuyt, and D. Van Dijck

EMAT, University of Antwerp (RUCA), Groenenborgerlaan 171, B-2020 Antwerpen, Belgium

J. Briers,‡ Ying Bao, and H. J. Geise*

University of Antwerp (UIA), Department of Chemistry, Universiteitsplein 1, B-2610 Wilrijk, Belgium

Received September 1, 1995; Revised Manuscript Received November 20, 1995[⊗]

ABSTRACT: The optimized synthetic procedures are given that lead to stretched poly(*p*-phenylenevinylene) (PPV) films of high molecular alignment and chemical homogeneity. Films of sulfonium precursor, pristine PPV, and $FeCl_3$-doped PPV are fully characterized spectroscopically as well as by electron microscopic and electron diffraction techniques. In particular, the paracrystalline structure of PPV is examined and the fluctuation values of the average cell edge vectors are measured; the values $\Delta_{11}(3) = \Delta_{22}(3) > 0.27$ Å and $\Delta_{33}(3) < 0.12$ Å were obtained. Furthermore, the molecular orientation in films of the precursor, the stretched pristine, and stretched, $FeCl_3$-doped phases is investigated. An angular distribution function about the stretching direction is measured and tested against the pseudo-affine (Kratky) deformation model.

Introduction

Among the π-conjugated polymers, poly(*p*-phenylenevinylene), abbreviated as PPV (see Figure 1), is somewhat special. The polymer has good thermal and air stability, is relatively easy to prepare, and can be doped by a number of dopants to high electrical conductivities.[1−5] Moreover, when prepared by the sulfonium precursor route,[6−8] thin, free-standing films can be made with excellent optical[9] and mechanical[2] properties. In our research to synthesize and characterize organic materials with potential in opto-electronic applications we optimized this route and now routinely make stretched films with a high molecular alignment. This induced us to perform a comprehensive electron microscopic study of PPV in order to confirm and to extend the pioneering studies of Karasz and co-workers.[2,8,10−15] Before, however, discussing the electron microscopic work, we will give a detailed account of the film preparation conditions, because they are crucial in determining the final alignment.

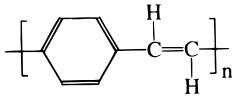

Figure 1. Structural formula of PPV.

Preparation Procedures

Figure 2 shows the steps involved in the preparation of the materials and films used in this work, together with their numbering.

The sequence starts with the synthesis of the bis(tetrahydrothiophenium chloride) salt **(2)**, the purity of which was established by capillary electrophoresis. Then, the monomer salt **(2)** is polymerized to the sulfonium precursor polymer **(3)**. Conditions, such as concentration of **2**, temperature (0 °C), and time (1 h) of polymerization, were optimized to avoid premature elimination of tetrahydrothiophenium side groups and to avoid gel formation. Dialysis, removing unreacted starting products, NaCl and oligomeric fraction, results in an aqueous solution of **3**, which is stable at 0 °C for 2−3 months. After casting the solution **(3)** onto a silanized glass surface, free-standing, flexible, yellowish-green precursor films **(4)** are obtained with a typical thickness of 10−12 μm. Freshly prepared, these films are completely soluble in water. Unfortunately, their stability is limited: spontaneous elimination

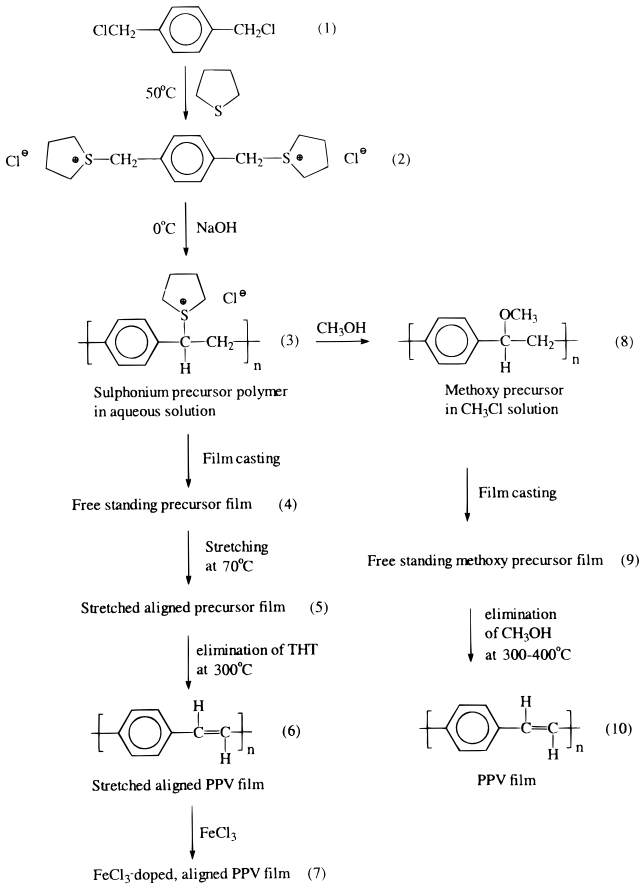

Figure 2. Steps involved in the preparation of the materials together with the numbering used in this work.

* To whom correspondence should be addressed.

† Present address: Department of Materials Science and Engineering, Zhejiang University, Hangzhou 310027, Zhejiang Province, P.R. China.

‡ Present address: 3M Belgium NV-SA, Canadastraat 11, 2070 Zwijndrecht, Belgium.

[⊗] Abstract published in *Advance ACS Abstracts,* January 15, 1996.

0024-9297/96/2229-1554$12.00/0

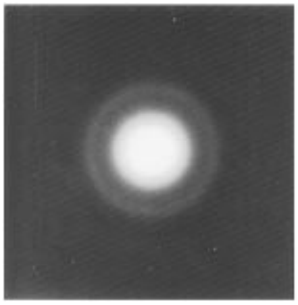

Figure 3. Electron diffraction pattern of a PPV-precursor film, **4**.

occurs at room temperature and is responsible for a decreasing water solubility with time. Despite all precautions elimination cannot be avoided completely at this stage. It shows for example in a blue fluorescence of solutions **(3)** and a yellow fluorescence of films **(4)**, visible under UV irradiation.

Preferably freshly prepared films **(4)** are then stretched under nitrogen at 100−120 °C. Obviously, under these conditions elimination progresses. This raises the glass transition temperature of the material, which in turn hinders the stretching alignment. Nevertheless, elimination also brings some benefits: particularly in the beginning of the process, stretching is helped by the plasticizing properties of the eliminating products. We found that the best results were obtained when we stretched films **4** to 4−8 times their original length in the shortest possible time and immediately continued to further process the films **(5)** formed.

Films **5** are converted to fully eliminated PPV films **(6)** in the all-trans configuration. Optimum conditions for the complete removal of sulfonium groups were established from thermogravimetric analysis in combination with in situ infrared spectroscopy. Elimination is complete and no C=O defects are introduced when the films are heated under nitrogen at 300 °C for 3 h. When such films are kept in air, some oxygen is absorbed (see Experimental Section), but this does not change the alignment. Infrared dichroic ratios measured on films **6** resulted[16] in a Hermans orientation value of $f = 0.96$.

Finally, stretched, $FeCl_3$-doped PPV films **(7)** are prepared. The conditions, such as concentration of $FeCl_3$ (0.12 M in nitromethane) and doping time (4 min) were selected for highest conductivity in the stretching direction (230 $\Omega^{-1}\cdot cm^{-1}$) and best tenability.[17] We end this section with two conclusions concerning PPV synthesis coming from coupled thermogravimetric−infrared experiments: (i) tetrahydrothiophenium is superior to dimethylsulfonium as a leaving group, and (ii) the sulfonium-precursor route is superior to the methoxy-precursor route[18,19] at least for the synthesis of PPV (see Figure 2). The first conclusion could be drawn when it was shown[17,20] that conversion of a dimethylsulfonium precursor film under optimum elimination conditions leaves more sulfur and more C(sp^3)−H defects in the final PPV film than does a precursor film **(4)**. To arrive at the second conclusion, we started from the methoxy-precursor polymer **8** (Figure 2) and observed[17,20] that even after heating to 420 °C the elimination of CH_3OH was incomplete and that even under strict nitrogen protection the introduction of C=O defects could not be avoided. It should be noted, however, that in contrast to PPV, the methoxy-precursor route is indeed an excellent route toward poly(2,5-dialkoxy-1,4-phenylenevinylene)[19,21,22] and toward poly(2,5-thienylenevinylene).[23]

Electron Diffraction of the Sulfonium Precursor Films, 4

Figure 3 shows the electron diffraction (ED) pattern of an unstretched PPV sulfonium-precursor film, **4**. No sharp reflections, only one diffuse ring, are seen, which indicates that the sulfonium-precursor polymer is amorphous and that its chains are homogeneously distributed without preferential orientation.

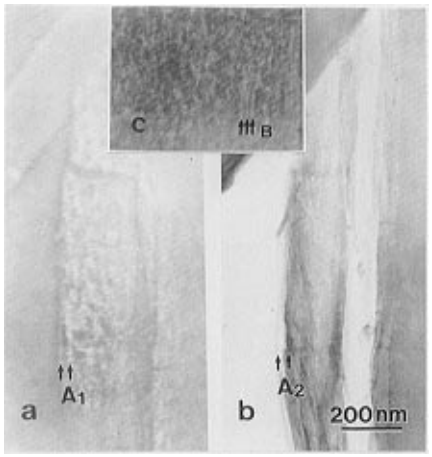

Figure 4. Central dark field image of films **6**, obtained from the 110/200 reflections, showing in (a) microfibers at A1 and in (c) microfibers at B. The bright field image obtained from the same area as (a) is given in (b).

The spacing corresponding to the periodicity of the diffuse ring is 0.23 nm in real space. It is indexed as the third-order reflection due to the repeat units in the precursor polymer, while the first- and second-order reflections are considered too weak to be observed. For this we use the following arguments. The precursor polymer has a backbone similar to that of PPV itself, the repeat unit of which has a length of 0.66 nm (see below) and an ED pattern in which the third layer lines also have a much higher intensity than the first and second layer lines. Then, it follows that the monomer length of the sulfonium precursor is 0.69 nm.

Electron Diffraction of Stretched PPV Films, 6

Dark Field Images. Parts a and c of Figure 4 give central dark field images obtained from the 110/200 reflections (see below) of a stretched ($l/l_o = 5$) PPV film **6**. Its bright field image is given in Figure 4b for comparison. The small reflecting areas, which have equal axes, can be considered to be crystalline regions with dimensions ranging from 3.5 to 10 nm, with an average size of about 6 nm. This compares very well with the results (12 and 7 nm) reported for PPV by Gagnon et al.[11] and Masse et al.,[14] respectively, and suggests that in PPV only small size crystallites exist. Furthermore, the fiber-like morphology can be seen at the positions A_1, A_2, and B in Figure 4. The diameter of the fibrils is 20−30 nm, which will be confirmed below by transmission electron photographs.

Electron Diffraction Patterns. Typical electron diffraction patterns of stretched ($l/l_o = 5$), pristine PPV films **6** taken under conditions of normal incidence are presented in Figure 5. The patterns—very similar to those published previously by Granier et al.[12]—are indexed (Table 1) as outlined before.[12] The spacing between the layer lines corresponds exactly to the repeat distance of 0.66 nm (the length of the monomer) along the PPV chains, as deduced from the crystallographic study of *trans*-stilbene by Finder et al.[24] Our results differ from those of Granier et al.[12] in that we observe nine instead of six layer lines, indicating a higher degree of order in our samples and resulting in slightly different lattice parameters (Table 1).

It may be noted that the features shown do not change significantly when the specimen is tilted about the fiber axis (*c*-axis in Figure 5), nor when more specimens were investigated. It proves that films **6** contain crystalline

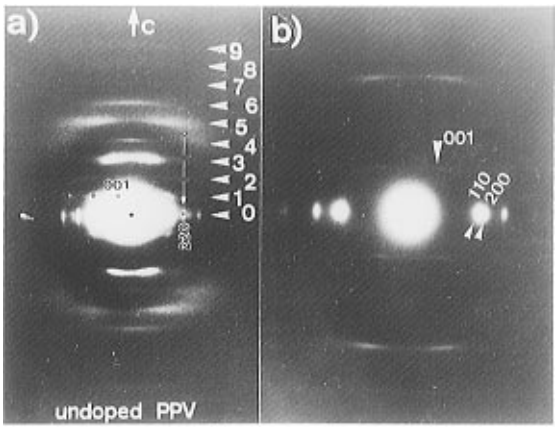

Figure 5. Electron diffraction pattern of PPV films **6**: (a) normal exposure; (b) showing an expansion of the central region of (a).

Table 1. Observed Reflections and Their Indexing in Electron Diffraction Patterns of Stretched PPV Films, *6*

d (Å)	intensity	index	lattice params
4.38	strong	110	$a = 8.1$ Å
4.03	strong	200	$b = 6.1$ Å
3.16	medium	210	$c = 6.6$ Å
2.37	medium	310	$\alpha = 123°$
2.17	weak	220	$\beta = \gamma = 90°$; $Z = 2$
1.89	medium	320; 410	observed layer lines: 9
1.56	weak	420; 510; 230	

regions and that the molecular chains are fully extended and well oriented.

Other useful information, in particular about the orientation function can be derived from the electron diffraction pattern by measuring the intensity distribution along the equatorial and the azimuthal direction. Figure 6 shows the results of these measurements, where Figure 6a gives the intensity distribution along the equator, from which the background intensity for the (210) reflection is measured and indicated as $I_{210}{}^{b}$ in Figure 6a. The azimuthal scan of the intensity of the (210) reflection is given in Figure 6b. After subtraction of $I_{210}{}^{b}$ a largest angular deviation of 17.7° and a full-width-at-half-height of 8.7° is obtained. Inserting the latter value as $\gamma = 8.7°$ into the Herman's orientation function[25−27] (eq 1) yields $f(\gamma) = 0.977$. The latter

$$f(\gamma) = 0.5(3\langle\cos^2\gamma\rangle - 1) \qquad (1)$$

value should be considered as a lower limit of the real value, because the result was obtained without taking into account other factors that broaden the intensity profile (e.g. finite crystallite size, deviations from uniform cylindrical symmetry of the fibers, paracrystalline lattice distortions, chain configurational disorder). The ED-profile value $f(\gamma) = 0.977$ is larger than that from measurements of the IR dichroic ratio ($f(\gamma) = 0.96$ (Table 2)) because the former value emphasizes the crystalline regions in which the chain molecules are regularly packed and thus better aligned than in the other, more disordered regions, such as grain boundaries or other amorphous phases. Like all vibrational analyses of oriented polymers, the dichroic ratio method provides a value for the molecular orientation that takes into account both crystalline and amorphous phases. We may interpret these data by starting from the consideration that our samples (films **6**) are composed of small crystallites of 5−7 nm. From 2H quadrupole echo NMR results[14,28] we take that about 50% of the sample volume is occupied by the crystallites while the remaining 50%

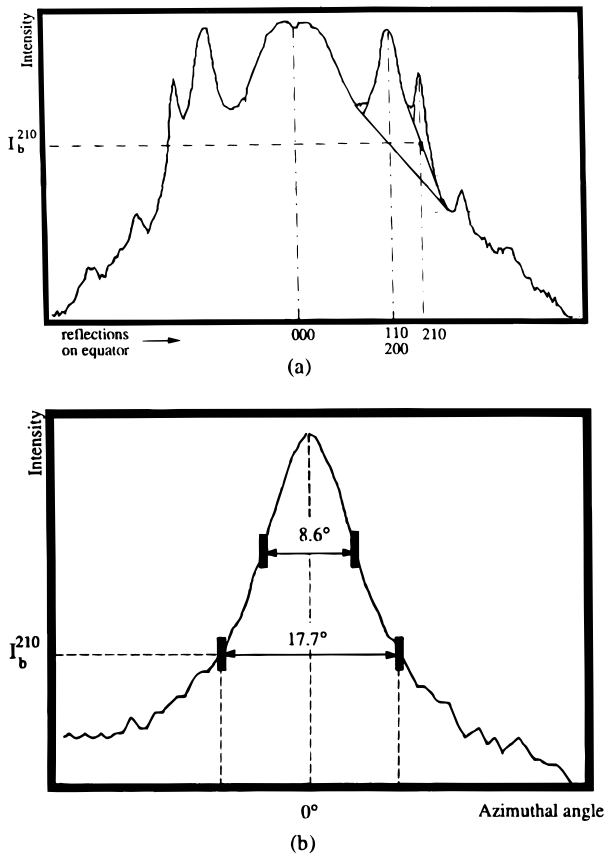

Figure 6. (a) Intensity scan along the equator (zeroth layer line) of the electron diffraction pattern shown in Figure 5b. Note the background intensity ($I_{210}{}^{b}$) measured for the 210 reflection. (b) Azimuthal intensity distribution of the 210 reflection, scanned from the same pattern as (a).

Table 2. Values of Hermans Orientation Function Determined by Various Methods

method	*f*	spread in γ (deg)	max angular deviation	source
IR dichroic ratio	0.96			ref 16
ED diffraction profile	0.966	8.6	17.7	this work
ED paracrystallinity	0.976	7.2		this work
TEM microfibrils	0.99	2.7	15	this work
high-resolution electron microscopy[a]	0.99			ref 14

[a] Measured on a different sample.

is thought to be grain boundaries. If we now take $f = 0.94$ (the smallest value found for fully stretched PPV) as an average for crystalline and "amorphous" rgions and $f = 0.97$ for the crystalline region, we arrive at $f = 0.91$ for the amorphous region. These f values correspond to an average misorientation $\gamma = 8°$ and $\gamma = 15°$ for the crystalline and "amorphous" regions, respectively. The small difference between these extremes ($\Delta\gamma = 7°$) strongly indicates that the 50% of the repeat units of the chain molecules which are supposed to exist in severely disordered regions of the grain boundaries is still well aligned in the stretching direction.

Paracrystalline Structure. Diffuse intensity layer lines are observed (Figure 5) in the electron diffraction pattern of films **6**, with streaks occurring along the direction perpendicular to the chain axis. This implies that PPV chains are not well registered along the chain axis; i.e. shifts exist between the chains. Such translational disorder and the corresponding intensity profiles may be consistently interpreted by the paracrys-

Table 3. Principal Values (Å) of Fluctuation Tensors in the Paracrystalline Lattice of PPV Films *6*

	$\Delta_{11}(1)$	$\Delta_{22}(1)$	$\Delta_{33}(1)$	$\Delta_{11}(2)$	$\Delta_{22}(2)$	$\Delta_{33}(2)$	$\Delta_{11}(3)$	$\Delta_{22}(3)$	$\Delta_{33}(3)$
previous work, ref 12	≤0.4	≤0.4	≥1.6	≤0.4	≤0.4	≈0.4	0[a]	0[a]	≤0.23
this work	≤0.4	≤0.4	≥1.6	≤0.4	≤0.4	≈0.4	>0.27	>0.27	≤0.12

[a] Assumed.

talline lattice model.[29] An ideal paracrystalline lattice is characterized by three fluctuation tensors, one for each of the cell edges. According to Wilke[30] the principal values (Δ_{ij}) of such a tensor with regard to a primitive lattice are given by

$$\Delta_{jj}^2(k) = \{\mathbf{e}_j(k)(\mathbf{x} - \mathbf{a}_k)\}^2 H_k(\mathbf{x}) d^3\mathbf{x} \qquad (2)$$

where $\mathbf{e}_j(k)$ represents orthogonal coordinate systems parallel to the directions of the principal axes, $\mathbf{a}_k$ the mean cell-edge vectors, $H_k(\mathbf{x})$ the cell-edge statistics, and $k = 1-3$ the cell direction indices. Assuming Gaussian functions for the statistics $H_k(\mathbf{x})$, Granier et al.[12] calculated the intensity profiles of a perfectly oriented, randomly shifted PPV system. Comparing our experimental intensities with the calculated profiles resulted in the confirmation of Granier's values for $\Delta_{11}(1)$, $\Delta_{22}(1)$, $\Delta_{33}(1)$, $\Delta_{11}(2)$, $\Delta_{22}(2)$, and $\Delta_{33}(2)$ (Table 3, ref 12).

The better registration in our samples of the PPV chains in the *c*-direction (nine layer lines instead of six; Figure 5) allows us to obtain more detailed information about $\Delta_{11}(3)$, $\Delta_{22}(3)$, and $\Delta_{33}(3)$.

We recall that these three parameters describe the mean square of fluctuations of $H_3(\mathbf{r})$, that is reflecting the deviations from periodicity of the chain molecules along the *c*-axis. An infinite straight chain of repeat distance *c* (Figure 7a) gives $H_3(\mathbf{r})$ the form of a δ-function: $H_3(\mathbf{r}) = \delta(\mathbf{r} - \mathbf{c})$ with $\Delta_{11}(3) = \Delta_{22}(3) = \Delta_{33}(3) = 0$. To estimate $\Delta_{11}(3)$ and $\Delta_{22}(3)$, one must consider the effects of misorientation of chain molecules due to bending or to local inclination of the molecules (Figure 7b). If the misorientation is slight, as it is in stretched PPV, $H_3(\mathbf{xyz})$ can be approximated by

$$H_3(xyz) = \delta(z - c)H_3'(xy) = \delta(z - c)D(\alpha) \qquad (3)$$

in which $H_3'(xy)$ gives the probability distribution of the ends of the *c*-vector in the plane $z = c$. The misorientation angle $\alpha = r/c$, where *r* is the polar radius in the plane $z = c$. If we assume that the bending or local misorientation is equally probable for all directions normal to the molecular axis, i.e. $\Delta_{11}(3) = \Delta_{22}(3) = \Delta_r$, further assume for the moment that $\Delta_{33}(3) = 0$, and use a Gaussian approximation to $H_3'(xy)$ then

$$H_3(xyz) = \delta(z - c)\frac{1}{2\pi\Delta_r^2}\exp\left\{-\frac{r^2}{2\Delta_r^2}\right\} \qquad (4)$$

with $r^2 = x^2 + y^2$. It is readily seen that the standard deviations of the *c*-vectors, i.e. the angular spread of $D(\alpha)$, are given by $\Delta(\alpha) = \Delta_r/c$ (Figure 7c). Since $H_3(xyz)$ has no spread *yet* in the *c*-direction, all layer planes will have the same form. The component $\Delta_r(\Delta_{11}(3),\Delta_{22}(3))$ is not zero, and thus the planes become diffuse as the radial coordinate *R* in the diffraction pattern along the *c*-axis increases. The critical radius R_c of the cylindrical region in which the planes remain visible is given[29,31−33] by

$$R_c\Delta_r = \frac{h_3}{\langle c\rangle}\Delta_r \approx 0.22 \qquad (5)$$

where *h* is the order of the last visible reflection and ⟨c⟩ the cell length in the *c*-direction. For PPV films **6**, $h_3 = 9$ and ⟨c⟩ = 6.6 Å, from which follows $\Delta_{11}(3) = \Delta_{22}(3) = \Delta_r = 0.42$ Å and $\Delta(\alpha) = 3.6°$. Hence, the full-width-at-half-height angle $\gamma = 7.2°$ and the value of $f = 0.976$. The relationship between Δ_r and *f* is given in Table 4. Next, we proceed to estimate the (very small) value of $\Delta_{33}(3)$.

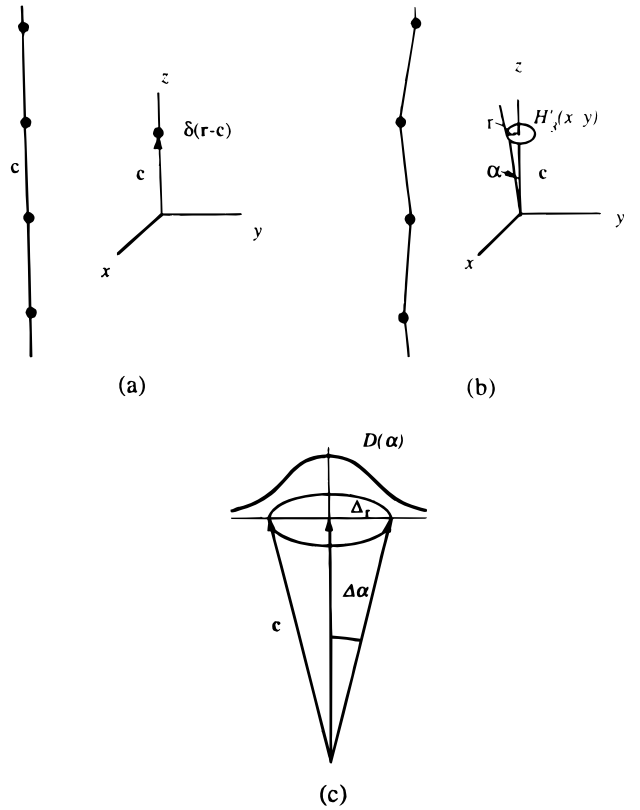

Figure 7. (a) Distribution function $H_3(\mathbf{r})$ for an ideal straight chain polymer with dots representing the monomeric units. (b) Statistics for a polymer with bending. (c) Distribution function $D(\alpha)$, describing the angular spread of vectors due to flexures in the polymer.

Table 4. Relation between the Hermans Orientation Function Values, *f*, and Deviations from Chain Periodicity, Δ_r

f	0.90	0.92	0.93	0.94	0.95	0.96	0.97	0.98	0.99	1.00
Δ_r	0.87	0.77	0.72	0.67	0.61	0.54	0.47	0.38	0.27	0

The three-dimensional analogue of eq 5 is

$$R_c^2\Delta_r^2 + (\Delta_{33}^2(3)h_3^2)/c^2 \approx [0.22]^2 \qquad (6)$$

From eq 6 and Table 4 it is clear that the lower limit of Δ_r determines the upper limits of $\Delta_{33}(3)$ as well as of *f*. Taking the upper limit of *f* as 0.99, we arrive at a lower limit of $\Delta_r = 0.27$ Å and an upper limit of $\Delta_{33}(3) \approx 0.12$ Å for stretched ($l/l_o = 5$) PPV films **6**.

Electron Microscopic Conservations of Stretched PPV Films, 6

Scanning electron micrographs of stretched and mechanically fibrillated PPV films **6** exhibit (Figure 8) microfibril surfaces along which long furrows run. It

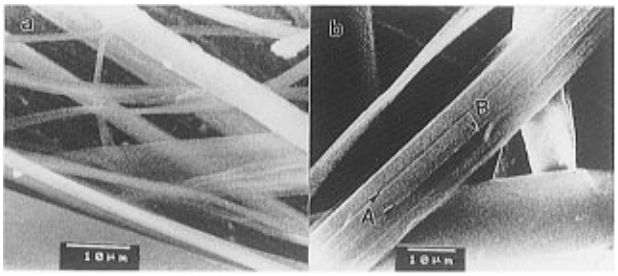

Figure 8. Scanning electron micrographs of PPV films **6** showing ribbons (at A) and furrows (at B) on the surface.

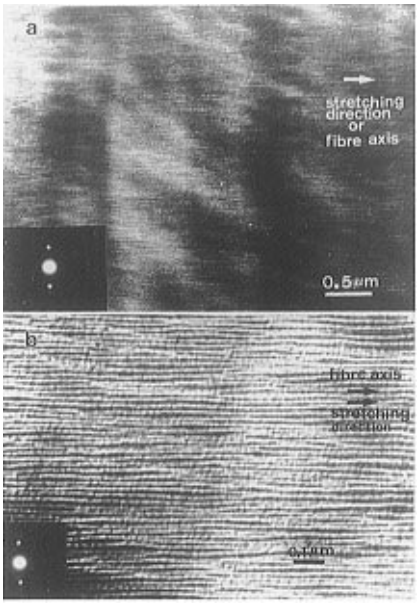

Figure 9. (a) Transmission electron micrograph of PPV film **6**, showing fibrils. (b) Higher magnification of (a). The insets show the diffraction pattern selected from this area.

follows that fibrillation occurs along the stretching direction, and hence parallel to the molecular chain. Transmission electron microscopic bright field images (Figure 9) of films **6** clearly also show that the fibrillar morphology with microfibrils is very well aligned in the stretching direction, just like in the SEM micrograph. Note that the microfibril diameters are all about 20 nm, in agreement with the dark field images.

To determine the degree of orientation, a statistical analysis of the fibril distribution about the stretch direction was carried out. To do so, we used seven micrographs (see Figure 9a for an example), each of which was divided into 70 squares, and the angular deviation, γ, of one fibril per square was measured with respect to one fibril direction in the micrograph chosen to represent the stretching direction (i.e. reference direction). The seven distributions, each containing 70 data points, were combined under the assumption that each should be centered around $\gamma = 0°$. In this way we (partly) randomized the systematic errors introduced by equating a particular fibril axis to the stretching direction. The histogram of the combined distribution (490 data points), given in Figure 10, suggests a residual centering error of 0.4°. Furthermore, it directly gives the value of the Hermans orientation function $f(\gamma) = 0.99$. From a high-resolution electron micrograph, Masse et al.[14] obtained the angular distribution of 27 individual crystallites in a PPV film with stretch ratio 9.3. From their data we arrive at $\langle \cos^2 \gamma \rangle = 0.885\ 60$ and $f(\gamma) = 0.99$.

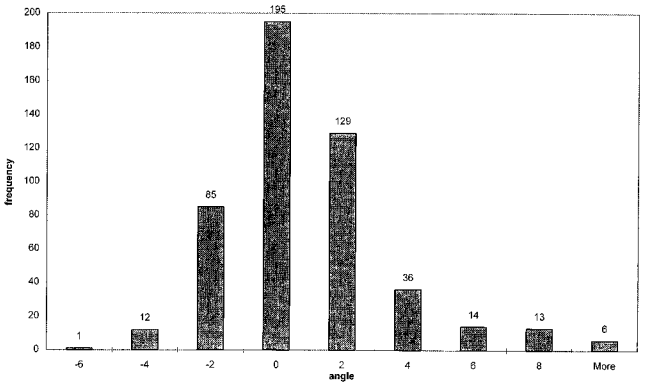

Figure 10. Histogram showing frequencies of angular deviations (deg) from stretching directions of microfibrils of PPV films **6**.

Hermans Orientation and Angular Distribution Function

The $f(\gamma)$ values determined by various methods are collected in Table 2. It should be noted that with the exception of the high-resolution electron microscopy (HREM) results[14] all measurements were performed on the same PPV films **6**.

The slightly higher values obtained by electron microscopic techniques compared to the one obtained by infrared follow from the electron microscopic sampling strategy. In fact the small regions selected for the measurements are crystalline and the region of the grain boundaries is excluded. Furthermore, values measured from fibril micrographs could be overestimated, because a straight appearance of a fibril does not imply that all composing chain molecules are strictly parallel to the fibril axis nor does it imply the absence of defects. In other words possible twists and inclinations of individual chain molecules are not visible. Nevertheless, the internal consistency of the results is so high that the angular distribution function of the fibrils (Figure 10) can be considered as a very good approximation of the angular distribution function of the chain molecules themselves. So, we proceed to compare this experimental distribution function with a Gaussian distribution and with the one derived from the pseudo-affine deformation (Kratky) model.[34−36] The least-squares fit to the Gaussian function

$$P(\gamma) = P(\gamma{=}0)\ \exp\{-(\gamma - p)^2/2\sigma^2\} \qquad (7)$$

gives $P(\gamma{=}0) = 195(8)$, $p = 0.4(1)°$, and $\sigma = 1.9(1)°$. It explains 98.9% (R^2) of the variance with an F-value of 218, well above the critical value for $F(2;5;0.01)$. Thus, the experimental data are normally distributed and centered around $\gamma = 0.4°$ (remaining centering error).

The least-squares fit to the Kratky distribution function

$$P(\gamma) = P(\gamma{=}0) \times \left\{ \frac{(l/l_o)^{3/4}}{[(l/l_o)^{3/2} \sin^2(\gamma - p) + (l/l_o)^{-3/2} \cos^2(\gamma - p)]^{3/2}} \right\} \qquad (8)$$

gives for the experimental stretching value $l/l_o = 5$, the parameter values $P(\gamma = 0) = 1.1(2)$ and $p = 0.4(9)°$. The fit, however, is poor, explaining only 71.5% of the variance with an F-value of 15.1, just above the critical value $F_{crit}(1;6;0.01) = 13.8$. When we add l/l_o to the adjustable parameters, one obtains an excellent fit explaining 98.9% of the variance and an F-value as high

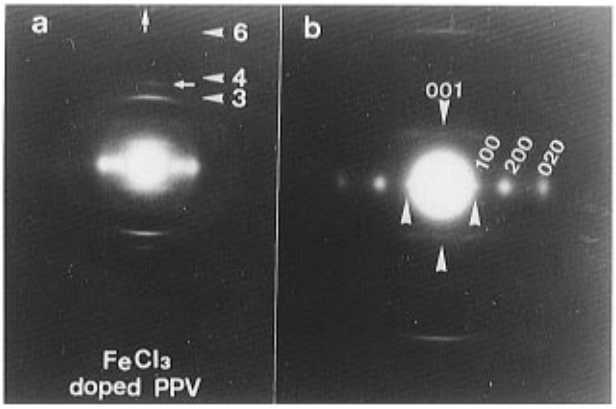

Figure 11. Electron diffraction patterns of $FeCl_3$-doped PPV films **7** showing (a) 6 layer lines (note the new meridional reflection between the third and fourth layer line) and (b) a new reflection, indexed as (001), as well as a different arrangement of lateral reflections on the zeroth line, compared to undoped PPV (Figure 5).

as 220.3 for the parameter values $P(\gamma=0) = 0.40(4)$, $p = 0.4(1)°$, and $l/l_o = 8.0(3)$, the last value being significantly higher than the experimental $l/l_o = 5$. This proves that the process of stretching during elimination of unoriented precursor films produces in PPV films an orientation significantly more efficient than that described by the pseudo-affine (Kratky) model. In other words, the pseudo-affine model overestimates the number of chain molecules at higher values of γ, i.e. those deviating more from the stretching direction. As such, our findings corroborate the conclusion of Bradley[37] and Simpson et al.[28]

$FeCl_3$-Doped Stretched PPV Films, 7

Figure 11 shows the electron diffraction patterns of $FeCl_3$-doped, stretched PPV films **7**. Evidently, the cylindrical symmetry about the *c*-axis remains unchanged compared to films **6**. One notes six layer lines, which have the same interspacing as in undoped PPV. This means that $FeCl_3$ doping does not change either the length of the monomers or the configuration or the orientation of the PPV chain molecules. The arrangement, however, of both longitudinal and equatorial reflections changes considerably. In Figure 11b, a new reflection, indexed as (001), appears on the *c*-axis, demonstrating a change from a monoclinic unit cell of the undoped crystal to an orthorhombic cell. At least one periodicity is observed along the first layer line, implying some extent of three-dimensional crystalline registry. On the zeroth layer only three equatorial reflections are visible, showing that the doped crystallites are highly imperfect. The latter reflections correspond to lateral spacings of 10.8, 5.4, and 3.3 Å and can be indexed as (100), (200), and (020) in an orthorhombic cell. The phase transition from the monoclinic to the orthorhombic unit cell upon doping PPV with other dopants was studied earlier by Masse et al.[13] Table 5 shows that the crystalline phases obtained with all dopants form a closely related family of electrically conducting structures. They all share the 3.3 Å (3.35 Å in $FeCl_3$) spacing and are indexed as the (020) reflection to give the length of the *b*-axis as 6.6 Å. On the other hand, the lattice parameter *a* is characteristic of the dopant used. Therefore, the 3.3 Å spacing may well be related to the lateral packing of the chain molecules themselves without notable interference from the dopant species. This spacing, being close to the 3.35 Å interlayer spacing in graphite, implies a planar packing of parallel PPV chains and supports a model in which stacked polymer chains are separated by planes containing dopant anions.

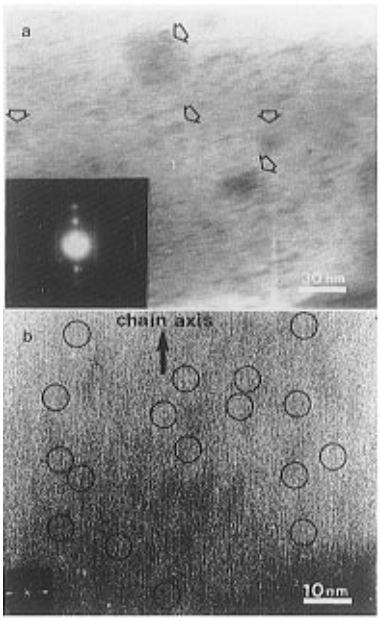

Figure 12. (a) High-resolution electron micrograph of $FeCl_3$-doped PPV film **7**, showing the electron dense area indicated by hollow arrows. The inset shows the small angle electron diffraction pattern of this image. (b) Higher magnification of the image (a) with the inset being the calculated Fourier transform of the image. The circled areas are considered as individual crystallites.

Table 5. Unit Cell Parameters of PPV Conductive Phases Obtained after Doping with Various Dopants

	dopant species (source)				
	$FeCl_3$ (this work)	H_2SO_4 (ref 13)	SbF_5 (ref 13)	AsF_5 (ref 13)	ClO_4^- (ref 13)
a (Å)	10.80	10.45	10.32	10.10	9.40
b (Å)	6.70	6.6	6.6	6.6	6.6
c (Å)	6.6	6.58	6.58	6.58	6.58

The slightly larger value of the *a*-axis length in $FeCl_3$-doped PPV (Table 5) probably reflects the larger Van der Waals radius of the $FeCl_4^-$ dopant anion intercalated in the complex. The nature of the dopant $FeCl_4^-$ was shown[38] by Mössbauer spectroscopy. It could not be inferred from the electron diffraction experiments, although a sign of it appeared in Figure 11a. The new meridional reflection between the third and fourth layer lines corresponds to a spacing of 0.18 Å along the *c*-axis, i.e along the polymeric chain in real space. Obviously, it is not produced by the polymer crystal, because it is incommensurable with the layer lines, and thus must be due to the dopant.

High-resolution electron micrographs of films **7** recorded with normal incidence show electron dense areas appearing as shadows (see Figure 12a). Even in these dense areas fringes with a spacing of 5.4 Å can be seen (Figure 12b). This spacing was confirmed from the pattern (shown in the inset of Figure 12b) generated after Fourier transformation of the image in real space. Unfortunately, no additional information could be extracted from this Fourier transformation pattern, since neither additional two-dimensional spots nor other high-order reflections were obtained.

Nevertheless, in the high-resolution image (Figure 12b) individual crystallites can be identified as regions

in which the fringes all have the same orientation as well as are all continuous both laterally and axially. Thus, relatively large regions displaying fringes can be divided into separate grains. The average domain size is about 50 Å, slightly smaller than that of undoped PPV (50−70 Å). Because of the small grain size, the grain boundaries between these crystallites must occupy a high percentage of the sample volume, just as they do in undoped PPV films of type **6**.

Conclusions

The polymer molecules in films of the sulfonium precursor of PPV do not show any preferential orientation. Molecular orientation is introduced upon uniaxial stretching and elimination.

Stretched ($l/l_o = 5$) PPV films are composed of microfibrils. From the high internal consistency of the Hermans orientation function measured by various methods, it is concluded that the angular distribution of the microfibrils about the stretch direction can be taken to represent the angular distribution function of the polymer chain molecules. It then follows that the stretching/elimination process produces in PPV films an orientation significantly more efficient than that described by the pseudo-affine (Kratky) model. An analysis based on the orientation measurements showed that grain boundary regions—having a lower value of the orientation function that that of the crystalline regions—are still composed of molecules well oriented along the fiber direction. These "disordered" regions, occupying about half the volume of the specimen, are easily doped and thus must play an important role in the doping process.

The paracrystalline structure of PPV is examined, and improved fluctuation values for the average cell-edge vectors are obtained.

High-resolution electron microscopic images and electron diffraction patterns of $FeCl_3$-doped (stretched) PPV show that the polymer chains keep the same orientation as in the undoped phase but that the spacing of the (200) planes increases from 4.0 to 5.4 Å and the monoclinic cell changes into an orthorhombic one. The doping process can be understood by a model in which doping $FeCl_4$ anions are intercalated between the polymeric chain molecules leading to a crystal−crystal phase transition.

Experimental Section

1,4-Phenylenebis(methyltetrahydrothiophenium chloride) (2). A mixture of 17 g (0.1 mol) of 1,4-bis(chloromethyl)-benzene and 26 g (26 mL, 0.3 mol) of tetrahydrothiophene in 100 mL of methanol was allowed to react at 50 °C for 24 h. Then, the solvent was partially evaporated to give a very viscous solution without precipitation of the salt **2**. The latter was precipitated by slow addition of cold (0 °C) acetone, then filtered off, washed with cold (0 °C) acetone, and dried in vacuo. Yield: 27 g (75%). The absence of a monosulfonium salt and of starting products in **2** was established by capillary electrophoresis.

FTIR: 3300−3200 cm^{-1} (remaining methanol); 3047 cm^{-1} (aromatic CH stretch); 3024 cm^{-1} ($C(sp^2)H$ stretch); 2920 cm^{-1} ($C(sp^3)H$ stretch); 1420^{-1} (CH_2SCH_2 bending). ^{13}C-NMR (in CD_3OD relative to tetramethylsilane): $\delta = 132.8$ (C_2 phenyl); $\delta = 132.5$ (C_1 phenyl); $\delta = 46.5(CH_2)$; δ 44.3 (C'_2 tetrahydrothiophene); $\delta = 29.6$ (C'_3 tetrahydrothiophene).

Tetrahydrothiophenium Precursor of Poly(phenylenevinylene) (3). A 0.2 M solution, prepared by dissolving 10 g (0.028 mol) of salt **2** in 150 mL of deionized water, was cooled to 0 °C. Then, an equimolar amount of a 0.5 M sodium hydroxide solution, prepared by dissolving 1.16 g (0.028 mol) of NaOH in 58 mL of deionized water, was dropped in over a period of 15 min. The mixture was stirred under nitrogen at 0 °C for 1 h. Occasional gel formation is prevented by addition of a small amount of deionized water. The polymerization reaction is quenched by adding 1 M hydrochloric acid until pH = 4−5.

The resulting, highly viscous polyelectrolyte solution is purified from residual monomer **2**, as well as from sodium chloride, tetrahydrothiophene, and low-molecular-weight oligomer by dialysis (using Visking membranes with a molecular weight cut-off of 3500) against deionized water for 5 days, replenishing the water three times per day. At the end of the dialysis chloride ions were no longer detected by $AgNO_3$.

The aqueous solution of **3** can be kept at 0 °C in a stoppered bottle for 2−3 months without visible deterioration.

Free-Standing Precursor Films (4). A silanized glass surface is prepared by washing a 20 × 20 cm glass plate successively with acetone, concentrated ammonia solution, methanol, toluene, a 0.5% solution of $(CH_3)_2SiCl_2$ in toluene, toluene, and methanol, followed by drying at 100 °C for 1 h. After cooling, the aqueous solution of **3** is poured onto the glass and water is allowed to evaporate at room temperature in a free air stream, avoiding dust as much as possible. After 24 h the very flexible, yellowish-green precursor film can be easily peeled off.

^{13}C-NMR using cross-polarization magic-angle-spinning: $\delta = 137.6$ (C_4 phenyl); $\delta = 132.5-130$ (C_1, C_2, C_3, C_5, C_6 phenyl); $\delta = 62.2$ (Ph−*C*H−); $\delta = 45$ (−*C*H_2−Ph, C_2, C_5 of tetrahydrothiophene rings); $\delta = 29.5$ (C_3, C_4 of tetrahydrothiophene rings).

Stretched Precursor Films (5). In an oven with a slight overpressure of nitrogen and preheated to 100−200 °C films **4** are stretched up to 8 times their original length. Exposition to oxygen is avoided to prevent the introduction of C=O defects in the polymeric chain and exposition to temperatures above 50−60 °C should be as short as possible to avoid elimination as much as possible at this stage.

Thermal Elimination to PPV Films (6). Films **4** or films **5** are heated under a nitrogen atmosphere at 300 °C for 3 h in which time complete elimination is achieved, as witnessed by the low percentages of sulfur and chlorine in the elemental analysis. Orange-brown, flexible films of all-trans PPV are obtained.

Anal. Calcd: C, 94.1; H, 5.9. Found: C, 91.0; H, 6.0; O, 2.51; S, 0.11; Cl, 0.26. IR: 965 cm^{-1} (trans CH=CH bending); 837 cm^{-1} (para-substituted phenyl). ^{13}C-NMR (cross-polarization magic-angle-spinning): $\delta = 137$ (C_1, C_4 phenyl); $\delta = 132$ (C_2, C_5 phenyl in ortho-anti position with respect to the vinylene link[39]; $\delta = 129$ ($C(sp^2)$ vinylene link); $\delta = 125$ (C_3, C_6 phenyl in ortho-syn position with respect to vinylene link[40]).

Stretched, $FeCl_3$-Doped PPV Films (7). PPV films **6** with stretch ratio $l/l_o = 5$ are doped under nitrogen protection in a 0.12 M solution of anhydrous $FeCl_3$ in dry nitromethane for 4 min, then washed thoroughly with dry nitromethane to remove unreacted $FeCl_3$ and produced $FeCl_2$, and finally dried in a dry nitrogen stream. The stretched, $FeCl_3$-doped PPV films, **7**, are stored under nitrogen at −20 °C.

Electron Microscopy and Sample Preparation. Small pieces (about 5 × 5 mm) are cut from a free-standing PPV film and fibrillated for scanning electron microscopic (SEM) examination. To obtain specimens for transmission electron microscopy (TEM), two techniques are used. In the one the film is embedded in an epoxy resin and sliced by a microtome into thin (100 nm) slices with the cutting plane parallel to the fiber axis. In the other technique, specially used for the stretched films, the specimen is fibrillated along the stretching direction using a sticky paper. The fibrils are then ultrasonically cleaned in chloroform. The fine pieces of the PPV fibrils are sandwiched between double copper grids for electron diffraction (ED) experiments, or deposited on holey carbon grids for high-resolution electron microscopic (HREM) observations.

A JSM-T220A scanning electron microscope was used to investigate the morphology, a JEOL 100C (operating at 100 kV) and a CM 20 TEM (operating at 200 kV) were employed for ED, bright field and dark field imaging, while a JEOL

200CX was employed for HREM. A lower accelerating voltage (120 kV instead of the usual 200 kV) was chosen and manual low dose operation was performed to minimize beam damage to the specimens during HREM operations. Computer-Fourier transformation was applied to confirm the HREM results, and graphite (0002) fringes (0.34 nm) were used to calibrate the camera constant.

To measure the optical density of an electron diffraction pattern, the negative photograph was scanned on an OFOTO APPLE ONE scanner, and the intensity distribution was analyzed on a Macintosh Quadra 900 computer by the program IMAGE.

Acknowledgment. This text presents research results of the Belgian Programme on Interuniversity Attraction Poles, initiated by the Belgian State (Primer Minister's Office), Science Policy Programming. Scientific responsibility, however, is assumed by the authors. Part of the work is performed with financial aid by the Flemish Ministery of Education (Contract Geconcerteerde Actie 89/94-10).

References and Notes

(1) Wnek, G. E.; Chien, J. C. W.; Karasz, F. E.; Lillya, C. P. *Polymer* **1979**, *20*, 1441.
(2) Gagnon, D. R.; Capistran, J. D.; Karasz, F. E.; Lenz, R. W. *Polym. Bull.* **1984**, *12*, 293.
(3) Murase, I.; Ohnishi, T.; Noguchi, T.; Hirooka, M. *Polym. Commun.* **1984**, *25*, 327.
(4) Gagnon, D. R.; Capistran, J. D.; Karasz, F. E.; Lenz, R. W. *Polym. Prepr. (Am. Chem. Soc., Div. Polym. Chem.)* No. 2, **1984**, *25*, 284.
(5) Murase, I.; Ohnishi, T.; Noguchi, T.; Hirooka, M. *Synth. Met.* **1987**, *17*, 639.
(6) Kanbe, M.; Okawara, M. *J. Polym. Sci., Polym. Chem. Ed.* **1968**, *6*, 1058.
(7) Wessling, R. A. *J. Polym. Sci., Polym. Symp.* **1986**, *72*, 55.
(8) Lenz, R. W.; Han, C. C.; Stenger-Smith, J.; Karasz, F. E. *J. Polym. Sci., Polym. Chem. Ed.* **1988**, *26*, 3241.
(9) Prasad, P. N.; Williams, D. J. *Introduction to Non-linear Optical Effects in Molecules and Polymers*; Wiley-Interscience: New York, 1991; pp 235 ff.
(10) Granier, T.; Thomas, E. L.; Gagnon, D. R.; Karasz, F. E.; Lenz, R. W. *J. Polym. Sci., Polym. Phys. Ed.* **1986**, *24*, 2793.
(11) Gagnon, D. R.; Karasz, F. E.; Thomas, E. L.; Lenz, R. W. *Synth. Met.* **1987**, *20*, 85.
(12) Granier, T.; Thomas, E. L.; Karasz, F. E. *J. Polym. Sci., Part B: Polym. Phys.* **1989**, *27*, 469.
(13) Masse, M. A.; Schlenoff, J. B.; Karasz, F. E.; Thomas, E. L. *J. Polym. Sci., Part B: Polym. Phys.* **1989**, *27*, 2045.
(14) Masse, M. A.; Martin, D. C.; Thomas, E. L.; Karasz, F. E.; Petermann, J. H. *J. Mater. Sci.* **1990**, *25*, 311.
(15) Machado, J. M.; Masse, M. A.; Karasz, F. E. *Polymer* **1989**, *30*, 1992.
(16) (a) Briers, J.; Eevers, W.; Cos, P.; Geise, H. J.; Mertens, R.; Nagels, P.; Zhang, X. B.; Van Tendeloo, G.; Herrebout, W.; Van der Veken, B. *Polymer* **1994**, *35*, 4569. (b) Simpson, J. H.; Egger, N.; Masse, M. A.; Rice, D. M.; Karasz, F. E. *J. Polym. Sci., Part B: Polym. Phys.* **1990**, *28*, 1859. (c) Nouwen, J.; Adriaensens, P.; Franco, D.; Vanderzande, D.; Martens, H.; Gelan, J.; Yang, Z.; Geise, H. J. *Synth. Met.* **1992**, *47*, 139.
(17) Briers, J. Ph.D. Thesis, University of Antwerpen, UIA, Belgium, 1993 (in Dutch).
(18) Momii, T.; Tokito, S.; Tsutsui, T.; Saito, S. *Chem. Lett.* **1988**, 1201.
(19) Halliday, D. A.; Burn, P. L.; Friend, R. H.; Bradley, D. D. C.; Holmes, A. B. *Synth. Met.* **1993**, *55*, 902.
(20) Yang, Z. Ph.D. Thesis, University of Antwerpen, Belgium, 1990.
(21) Tokito, S.; Smiths, P.; Heeger, A. J. *Polymer* **1991**, *32*, 464.
(22) Delmotte, A. Ph.D. Thesis, Free University Brussels, Belgium, 1993 (in Dutch).
(23) Eevers, W. Ph.D. Thesis, University of Antwerpen, UIA, Belgium, 1993 (in Dutch).
(24) Finder, C. J.; Newton, M. G.; Allinger, N. L. *Acta Crystallogr.* **1974**, *B30*, 411.
(25) Hermans, P. H.; Platzek, P. *Kolloid-Z.* **1939**, *88*, 68.
(26) Hermans, P. H. *Contributions to the Physics of Cellulosic Fibers*; Elsevier: Amsterdam, 1946; p 138.
(27) Siesler, H. W.; Holland-Moritz, K. In *Infrared and Raman Spectroscopy of Polymers*; Brame, E. G., Jr., Ed.; Practical Spectroscopy Series; Marcel Dekker, Inc.: New York, 1980; Vol. 4, Chapter 4.
(28) Simpson, J. H.; Rice, D. M.; Karasz, F. E. *Macromolecules* **1992**, *25*, 2099.
(29) Hosemann, R.; Bagchi, S. N. *Direct Analysis of Diffraction by Matter*; North-Holland: Amsterdam, 1962; pp 239−246, 654 ff.
(30) Wilke, W. *Acta Crystallogr.* **1983**, *A39*, 864.
(31) Bonart, R.; Hosemann, R.; McCullough, R. L. *Polymer* **1963**, *4*, 199.
(32) Bonart, R.; Hosemann, R. *Kolloid-Z., Z. Polym.* **1962**, *186*, 16.
(33) Alexander, L. E. *X-Ray Diffraction Methods in Polymer Science*, reprint ed.; R. E. Krieger Publishing Co. Inc.: Malabar, FL, 1985; Chapter 7.
(34) Kratky, O. *Kolloidn. Zh.* **1933**, *64*, 401.
(35) Zbinden, R. *Infrared Spectroscopy of High Polymers*; Academic Press: New York, 1964.
(36) Hardley, D. W.; Ward, I. M. In *Structure and Properties of Oriented Polymers*; Ward, I. M., Ed.; J. Wiley & Sons: New York, 1975; p 264.
(37) Bradley, D. D. C. *J. Phys. D.: Appl. Phys.* **1987**, *20*, 1389.
(38) Briers, J.; Eevers, W.; De Wit, M.; Geise, H. J.; D'Olieslagers, W.; Wauters, J.; Van Bavel, A. M.; Bemelmans, H.; Langouche, G. *J. Phys. Chem.* **1995**, *99*, 12971.
(39) Nouwen, J.; Vanderzande, D.; Martens, H.; Gelan, J.; Yang, Z.; Geise, H. J. *Synth. Met.* **1992**, *46*, 23.
(40) Nouwen, J.; Adriaensens, P.; Franco, D.; Vanderzande, D.; Martens, H.; Gelan, J.; Yang, Z.; Geise, H. J. *Synth. Met.* **1992**, *47*, 239.

MA9513067